Published in final edited form as:
J Immunol. 2012 November 1; 189(9): 4258–4265. doi:10.4049/jimmunol.1101855.

Depletion of plasmacytoid dendritic cells inhibits tumor growth and prevents bone metastasis of the breast cancer cells

Anandi Sawant[1], **Jonathan A. Hensel**[1,2], **Diptiman Chanda**[1], **Brittney A. Harris**[1], **Gene P. Siegal**[1], **Akhil Maheshwari**[3,4], and **Selvarangan Ponnazhagan**[1,*]

[1]Department of Pathology, University of Alabama at Birmingham, Birmingham, AL 35294

[3]Department of Pediatrics, University of Alabama at Birmingham, Birmingham, AL 35294

Abstract

Elevated levels of plasmacytoid dendritic cells (pDC) have been reported in breast cancer patients, the significance of which remains undefined. Using three different immunocompetent mouse models of BCa bone metastasis, we identified a key role for pDC in facilitating tumor growth through immunosuppression and aggressive osteolysis. Following infiltration of macrophages upon breast cancer dissemination, there was a steady increase of pDC within the bone, which resulted in a sustained Th2 response along with elevated levels of Treg and MDSC. Subsequently, pDC and $CD4^+$ T cells, producing osteolytic cytokines, increased with tumor burden causing severe bone damage. Micro-CT and histology analyses of bone showed destruction of femur and tibia. Therapeutic significance of this finding was confirmed by depletion of pDC, which resulted in decreased tumor burden and bone loss by activating tumor-specific cytolytic $CD8^+$ T cells and decreasing suppressor cell populations. Thus, pDC depletion may offer a novel adjuvant strategy to therapeutically influence breast cancer bone metastasis.

Keywords

Tumor immunity; Dendritic cells; Monocytes/Macrophages; Th1/Th2; Cytokines

INTRODUCTION

Nearly 80–90% of breast cancer patients with advanced disease have osteolytic disease, characterized by increased bone damage resulting from enhanced osteoclast activity (1). The presence of such bone lesions usually signifies serious morbidity and a grave prognosis with severe pain, pathological fractures, nerve compression syndromes and hypercalcemia (2). Current therapies for bone metastasis in breast cancer patients are limited and are focused only on symptomatic management, limiting the progression of established disease (3). Although a significant amount of research has been carried out on understanding breast cancer bone metastasis, not much is known about the events leading to the bone metastasis. Hence, a better understanding of the molecular mechanisms involved in the formation and progression of bone metastases is needed.

Dissemination of the primary tumor to the bone triggers the production of osteolytic cytokines and growth factors that result in osteoclast activation and promote tumor growth

[*]Corresponding author: Selvarangan Ponnazhagan, Ph.D., Department of Pathology, 701 19th Street South, LHRB 505, The University of Alabama at Birmingham, Birmingham, AL 35294-0007, Phone: (205) 934-6731; Fax: (205) 975-9927, pons@uab.edu.
[2]Current address: University of Colorado Denver, Denver, CO 80217
[4]Current address: Department of Pediatrics, University of Illinois, Chicago, IL 60612

and immune-suppression in the bone microenvironment (4). Conversely, products of bone cells are critical for normal development of the hematopoietic and immune systems (4). In osteopenic conditions like osteoporosis, bone destruction results from enhanced osteoclast activity with a concomitant decrease in osteoblast numbers, without a significant alteration in the immune system (5). But the osteolytic bone changes observed in bone metastasis are triggered by a coordinated interplay of bone homing cancer cells, osteoclasts and the immune cells in the bone marrow (BM) (6). Thus, elucidation of the molecular mechanisms during these interactions should provide new insights into the treatment for cancer bone metastasis.

Using immunocompetent mouse models of breast cancer dissemination to bone and other organs, the present study characterized the immune mechanisms that regulate osteolytic breast cancer metastasis at different stages of tumor progression. Results indicated that the vicious cascade promoting tumor growth, immune-suppression and bone damage is regulated by plasmacytoid dendritic cells (pDC), shifting the T helper cell (Th) homeostasis greatly towards the Th2 phenotype, independent of the effects of myeloid suppressor cells. Depletion of pDC *in vivo* resulted in a significant increase in Th1 response, leading to a decrease in both tumor growth and bone damage. Further, such a reversal of Th2 to Th1 response resulted in an increased $CD8^+$ T cell activity against the tumor in bone and visceral organs. Collectively, these data indicate the potential of this strategy for advanced stage breast cancer patients to decrease bone morbidity and increase survival.

MATERIALS AND METHODS

An *in vivo* model for breast cancer bone metastasis

Mouse breast cancer cell lines 4T1, constitutively expressing firefly luciferase [4T1(fLuc)], TM40D and r3T were kind gifts from Dr. Xiaoyuan Chen (Stanford University), Dr. Andre Lieber (University of Washington), and Dr. Susan Rittling (Forsyth Institute), respectively and cultured as described before (7–9). Approximately, 10^5 cells from each cell line were injected via the intra-cardiac route in respective syngeneic, female mice of 6–8 weeks of age (Frederick Cancer Research and Development Center, Frederick, MD). Progression of the 4T1 tumor growth and dissemination to the bone was followed by non-invasive imaging of mice using the IVIS Imaging System (Xenogen Corp.). On days 3, 7, 10 and 14, cohorts of mice were sacrificed for analyses. Blood was collected and serum separated. Selected visceral organs and bones were collected for histology. Spleen and BM were used for enumerating the immune cell profile and activation status. Tumor progression was also assessed in an interferon alpha receptor knock-out mouse model ($IFNAR^{-/-}$) in BALB/c background (kindly provided by Dr. Andrew Mellor, Georgia Health Sciences University) and in C57BL/6 background using a syngeneic osteolytic cell line.

Immune cell depletion

To deplete pDC, mice were injected intra-peritoneally with 250 μg of PDCA-1 antibody (clone # JF05-IC2.41; Miltenyi Biotec, Auburn, CA) every other day (10). As a control, mice were injected with similar amounts of IgG antibody (Miltenyi Biotec, Auburn, CA). Four days after injection of antibodies, blood was collected by retinal bleeding. Mononuclear cells obtained by Ficoll-Hypaq (GE Healthcare, Piscataway, NJ) gradient extraction were incubated with PDCA-1-Alexa 647 antibody (eBioscience, San Diego, CA) for 30 min and were enumerated by flow cytometry. Once depletion of pDC was confirmed, mice were challenged with 10^5 4T1(fLuc) cells by intra-cardiac route. Injection of PDCA-1 or IgG antibodies was continued until the end of the experiment.

Micro-CT and histology

Upon sacrifice of tumor-challenged mice at different time points, both femur and tibia were collected and fixed in 4% buffered-formalin for 2 days and were subjected to micro-CT analysis (Micro- CT40; SCANCO Medical, Wayne, PA). The formalin-fixed bones were then decalcified in 2.5% EDTA, pH 8.0, for 2 weeks. Five μm paraffin-embedded sections were used for histological analysis.

Immunohistochemistry

The presence of breast cancer cells in the visceral tissues and bone was detected by conventional light microscopic evaluation of H&E stained tissue sections by a senior anatomic pathologist and confirmed by staining with cytokeratin-8 antibody (Abcam, Cambridge, MA) as described previously (11). The presence of osteoclasts within the bone sections was detected by tartarate-resistant acid phosphatase (TRAP) staining as described previously (12). All the microscopic images were obtained using Leica DMI4000B microscope, attached to a Leica DFC500 digital camera. The LASv3.6.0 software was used to optimize picture quality and also for generating scale bars for individual images.

Isolation of immune cells and FACS analysis

Immune cells were isolated from the bone of tumor challenged mice. Both femur and tibia were flushed to collect bone marrow cells. Following RBC lysis using the ACK lysis buffer (Quality Biologicals Inc., Gaithersburg, MD), cells were suspended in FACS staining buffer (PBS + 2% FBS + 0.01% sodium azide) and incubated with Fc-Block, for 15 min at 4°C. These cells were stained (10^6 cells/group) to detect various immune cell populations using cell specific fluorescence conjugated antibodies, purchased from ebioscience, San Diego, CA, for 30 min at 4°C. Upon fixation with 4 % paraformaldehyde, cells were enumerated using a FACS Caliber Flow Cytometer (Beckman Coulter, Hialean, FL) (13). Thirty × 10^3 events were acquired for each sample. The data were analyzed using FlowJo software. For detecting the presence of Treg cells, cells stained with antibodies to CD3 (Clone 17A2), CD4 (Clone GK1.5) and CD25 (Clone PC61.5) were permeabilized with a commercially available permeabilization buffer (eBioscience, San Diego, CA), for 30 min, at 4°C and then stained with antibody to Fox-P3 for 30 min at 4°C. Within the $CD3^+CD4^+$ cells, subset of $CD25^+FoxP3^+$ cells was detected. These cells were considered as Treg.

For detecting the presence of PDCA-1 antigen on the 4T1(fLuc) cells, bone marrow cells were collected upon sacrifice of mice with established breast cancer bone metastasis. Following Fc-block, cells were stained with antibodies to CD45 (Clone 30-F11) and PDCA-1 (Clone eBio927) for 30 min at 4°C. Cells which stained negative for both the antibodies were sorted and cell lysate was prepared. Luciferase assay was carried out as per the manufacturer's instructions (Promega). As a control, 4T1(fLuc) cells grown *in vitro* were used for the luciferase assay.

Co-culture assay for osteoclast activity

For isolation of monocytes, cells were incubated with biotinylated CD115 antibody (eBioscience, San Diego, CA), for 15 min, at 4°C followed by incubation with anti-biotin microbeads (Miltenyi Biotec, Auburn, CA). Magnetic separation was carried out as per the manufacturer's instructions. For isolation of $CD4^+$ T cells, a commercially available kit was used (Miltenyi Biotec, Auburn, CA). Monocytes and $CD4^+$ T cells were cultured at a ratio of 1:100 where monocytes were plated in 96-well tissue culture plates (Corning Inc., Corning, NY) and $CD4^+$ T cells were placed in 0.2 μm tissue culture inserts (Nalge Nunc International, Rochester, NY). Media was changed as described previously (14). For determining the role of RANKL and IL-15 in osteoclast generation, recombinant OPG (100

ng/ml) and/or IL-15 antibody (10 μg/ml) was added in the co-culture either individually or in combination. After 10 days, presence of osteoclasts was detected by TRAP staining.

Cytokine assay

RNA was isolated from $CD4^+$ T cells by the TRIZOL RNA extraction method (Invitrogen, Carlsbad, CA). cDNA was prepared as per the manufacturer's instructions (Bio-Rad Labs., Hercules, CA) and was used in real-time RT-PCR assays for detecting the presence of cytokines IL-3, IL-6, IL-10, IL-11, IL-12, IL-15, IL-17, TGF-β and RANKL.

Serum cytokine levels were assayed using a commercially available Mouse 22-plex cytokine assay kit obtained from Millipore (Millipore Inc., Billercia, MA). Each assay was performed in triplicate.

Cytotoxicity assay

$CD8^+$ T cells were isolated from the BM using a commercially available $CD8a^+$ T cell isolation kit II (Miltenyi Biotec, Auburn, CA) and were used as the effector cells (E). 4T1(fLuc) cells were used as the target population (T). The assay was set up with E:T ratios of 5:1, 10:1, 20:1 and 40:1. The cytotoxicity assay was performed using the commercially available LIVE/DEAD cell-mediated cytotoxicity kit (Molecular Probes, Eugene, OR).

Statistical analysis

Data are presented as mean ± SE. Statistical analysis was performed using the Student's *t*-test. Statistical significance was determined at < 0.05 level.

RESULTS

An *in vivo* model of breast cancer bone dissemination

For understanding possible mechanisms that are conducive for the growth of breast cancer in the bone, we employed three different models with syngeneic breast cancer cell lines 4T1(fLuc) cells in BALB/c; r3T cells in 129S and TM40D cells in BALB/c mice. These cells upon intracardiac injection readily metastasized to various organs including the bone (Fig. 1a). Histologic analysis verified the presence of cancer cells in the liver and lungs (Fig. 1b) and in the tibia and femur (Fig. 1c). Micro-CT analysis of the tibia and femur, 14 days after tumor challenge, showed a dramatic destruction of bone compared to age-matched controls (Fig. 1d and Fig. S1) with increased osteoclast numbers (Fig. 1e).

Dissemination of cancer cells to the bone initiates an inflammatory reaction followed by pDC enrichment

As tumor cells disseminated to the bone, cohorts of mice were sacrificed and cells were collected from the BM to examine the profile of immune cells mediating the disease pathology. Results indicated that as breast cancer disseminated to the bone, there was an initial macrophage infiltration (Fig. 2a) followed by an increase in the $B220^+CD11c^+$ (Clone RA3-6B2 for B220 and Clone N418 for CD11c antibody) pDC population (Fig. 2b). To further confirm pDC specifically, $B220^+CD11c^+$ cells were stained for markers including SinglecH (Clone eBio440c), PDCA-1 and Gr-1. Close to or more than 90% of the $B220^+CD11c^+$ cells were positive for these markers, confirming the pDC increase in the bone (Fig. 2c).

Increased pDC numbers with increased bone metastasis was observed in all three models, confirming that elevated pDC numbers during progressive stages of breast cancer dissemination is not due to the variability (Fig. 2d and e).

Elevation of pDC numbers is accompanied by skewing of immune response towards Th2

Next, the effect of elevated pDC levels on T cell immune response was analyzed by characterizing the T-helper response in BALB/c mice with 4T1(fLuc) cells. Results of this study indicated significantly high levels of IL-4 compared to IFN-γ levels that progressed with tumor growth and bone metastasis, thus indicating a skewing towards Th2 response as the cancer progressed to invade and proliferate within the bone (Fig. 3a). The multiplex cytokine analysis from the sera of mice revealed an increased secretion of Th2 specific cytokines; IL-5 and IL-6 and reduced levels of Th1 specific IL-12 and IP-10 (data not shown). The switch to Th2 response also correlated with increased pDC levels.

As pDC skew the immune response towards a Th2 phenotype via a CD40-CD40L interaction in the presence of IL-3 (15), we examined the surface expression of CD40 (Clone 1C10) on pDC and CD40L (Clone PC61.5) on $CD4^+$ T cells. The skewing of the immune response towards the Th2 phenotype correlated with increased expression of CD40 and CD40L on pDC and $CD4^+$ T cells, respectively (Fig. 3b). IL-3 levels were elevated in $CD4^+$ T cells (Fig. 3c). Together, these data show that elevated pDC in the bone microenvironment polarizes the immune response towards a suppressive Th2 phenotype that allows tumor growth and spread into bone.

Increased production of osteolytic cytokines leads to increased osteoclast numbers and bone destruction

Cytokine analysis by the multiplex assay using sera from mice indicated a significant increase in the levels of IL-15, RANTES and MCP-1, known inducers of osteoclasts, as cancer dissemination progressed into and within the bone (Fig. S1). As $CD4^+$ T cells are a major source of osteolytic cytokines, we assayed for the presence of these cytokines in $CD4^+$ T cells from the BM of tumor-challenged mice. Our data indicated significantly higher levels of IL-6, IL-11, and IL-15 with increased bone destruction (Fig. 4a). We next determined if the increased cytokine production by $CD4^+$ T cells resulted in increased osteoclast numbers. To assay for osteoclast numbers, $CD4^+$ T cells, isolated from either spleen or BM, were co-cultured with BM-derived monocytes. Results indicated significantly high numbers of osteoclasts by TRAP staining when monocytes were co-cultured with BM-derived $CD4^+$ T cells compared to those from spleen (Fig. 4b). Further, the number of osteoclasts increased as breast cancer metastasized within the bone.

We next determined if the $CD4^+$ T cells in the BM of tumor-bearing mice are more primed to effect monocyte differentiation into osteoclasts. For this purpose, monocytes from control mice were co-cultured with $CD4^+$ T cells from tumor-challenged mice, and monocytes from the tumor-challenged mice with $CD4^+$ T cells from control mice. Results indicated a significant increase in osteoclast numbers when $CD4^+$ T cells from tumor-bearing mice were co-cultured with monocytes either from tumor-challenged mice or from control mice (Fig. 4c). Conversely, $CD4^+$ T cells from control mice induced lesser numbers of osteoclasts when cultured with tumor-derived monocytes. However, osteoclast numbers were still significantly higher than that obtained after culturing monocytes and $CD4^+$ T cells from control mice suggesting that monocytes from tumor-challenged mice are more primed towards osteoclast differentiation.

Further, to determine which osteolytic cytokines played a major role in osteoclast activation, osteoprotegerin (OPG), a soluble decoy receptor of RANKL, and antibody to IL-15 were added to the culture either individually or in combination. Results of this study indicated that the number of osteoclasts was considerably reduced when OPG and IL-15 antibodies were added individually or in combination (Fig. 4d), confirming that both RANKL and IL-15 induce monocyte differentiation towards osteoclasts.

Depletion of pDC *in vivo* results in reduced tumor growth and absence of bone metastasis

In order to confirm that pDC are key regulators of breast cancer bone metastasis, pDC depletion was performed *in vivo* with PDCA-1 antibody (Fig. S2). As a control, cohorts of mice received isotype IgG antibody. On day-12 post tumor challenge, tumor growth was observed in the bones of both naïve (challenged with 4T1 cells but without any antibody treatment) and IgG injected mice. However, PDCA-1 injected mice not only showed a dramatic reduction in overall tumor burden (Fig. 5a & b), but the tumor cells did not disseminate to bone (Fig. 5a). Metastasis to lungs was significantly less compared to naïve and IgG injected groups (Fig. 5c & d). Cytokeratin-8 staining did not reveal the occult presence of cancer cells in the tibia of PDCA-1 injected mice, further supporting the luciferase image analysis (Fig. 5e).

To rule out the possibility that reduced tumor burden in PDCA-1 injected mice was not due to binding of the PDCA-1 antibody to 4T1(fLuc) cells, which could have prevented their proliferation, 4T1(fLuc) cells isolated from tumor-bearing mice were tested for their ability to bind to PDCA-1 antibody. Once breast cancer bone metastasis was established in mice, the animals were sacrificed and bone marrow cells were collected. Cells were stained for antibodies to CD45 and PDCA-1. As non-immune cells do not express CD45, staining for PDCA-1 was detected among $CD45^-$ cells. Results clearly indicated an absence of PDCA-1 staining on $CD45^-$ cells. Further, to confirm that the $CD45^-$ cells that did not bind to PDCA-1 were indeed 4T1(fLuc) cells, these cells were sorted and luciferase activity was determined in that population since the 4T1(fLuc) cells used in this study constitutively expressed firefly luciferase. High luciferase count was detected suggesting that a major fraction of $CD45^-PDCA\text{-}1^-$ cells were indeed breast cancer cells (Fig. S2). This observation confirmed that *in vivo* breast cancer cells isolated from the bone microenvironment do not express PDCA-1, thus eliminating any direct effect of PDCA-1 antibody treatment on tumor growth and dissemination and validating its use for this study.

For further direct confirmation that pDC indeed play a vital role in breast cancer bone metastasis, a genetic mouse model lacking expression of interferon alpha receptor ($IFNAR^{-/-}$) was used as these mice lack functional pDC (16, 17). A similar study in this model showed a dramatic reduction in the growth of breast cancer in $IFNAR^{-/-}$ mice compared to the syngeneic WT mice thus confirming a role for pDC in promoting tumor growth and metastasis (Fig. 5f).

Micro-CT analysis of femur and tibia following PDCA-1 injection did not show bone destruction as seen in the naïve and IgG injected mice (Fig. 6a), which also correlated with less $TRAP^+$ osteoclasts in tibia (Fig. 6b). These results were further confirmed when upon co-culture of $CD4^+$ T cells and monocytes, PDCA-1 group had significantly less numbers of osteoclasts compared to the naïve and IgG groups (Fig. 6c). The decreased osteoclast numbers can be attributed to decreased amounts of osteoclast-inducing cytokines in mice treated with PDCA-1 antibody (Fig. 6d, Fig. S3). Similar to results observed in PDCA-1 group, micro-CT analysis also revealed reduced bone destruction in tumor-challenged $IFNAR^{-/-}$ mice compared to the WT mice (Fig. 6e). Together, these data demonstrate that pDC enhance breast cancer bone metastasis.

Additionally, to rule out the possibility that the genetic background of $IFNAR^{-/-}$ mice (BALB/c) played a role in reduced tumor growth and osteolysis, similar study was also carried out in $IFNAR^{-/-}$ mice in C57BL/6 background using an osteolytic cell line. Data clearly demonstrated that the genetic background of $IFNAR^{-/-}$ mice did not affect outcome of results as reduced tumor growth and osteolysis was also observed in $IFNAR^{-/-}$ mice in C57BL/6 background (Fig. S4).

Depletion of pDC restores a Th1 type immune response

We next analyzed the effect of pDC depletion on the anti-tumor immunity. As expected, the numbers of pDC were markedly reduced in PDCA-1 injected mice compared to naïve and IgG injected mice (Fig. 7a). Decreased pDC levels resulted in an increase in Th1 cells with concomitant decrease in Th2 cells as assessed by high IFN-γ and low IL-4 levels respectively in PDCA-1 antibody injected group (Fig. 7b). But in both naïve and IgG antibody injected mice, elevated Th2 cells were seen as observed before. Multiplex cytokine analysis further supported the immune profile, showing increased secretion of Th1-associated cytokines (Fig. S3). Depletion of pDC also resulted in a decrease in MDSC and Treg numbers compared to naïve and IgG injected mice (Fig. 7c & d). To determine the possible mechanism for reduced tumor growth in pDC-depleted mice, $CD8^+$ T cells were isolated and used in cytotoxicity assay. Freshly isolated $CD8^+$ T cells from pDC-depleted mice exhibited significantly enhanced cytotoxicity compared to those from naïve and IgG groups against 4T1 cells as the target population (Fig. 7e).

We also detected pDC levels in bone marrow of WT and $IFNAR^{-/-}$ mice after tumor challenge. Unlike, elevated pDC levels observed in WT mice, $IFNAR^{-/-}$ mice did not exhibit such high pDC levels (Fig. 7f). This observation is concomitant with low pDC levels observed in PDCA-1 antibody injected group. Both these groups of mice also show drastically reduced breast cancer growth and bone metastasis.

DISCUSSION

Studies using tissues from human breast cancer patients have documented infiltration of pDC at the periphery of tumor and at sites of metastasis (18, 19). Plasmacytoid DC are also present in lymph nodes carrying breast cancer metastasis (20). However, the significance of this is not clearly defined. Using metastatic models of breast cancer in immunocompetent mice, the present study first established and then systematically defined these events connecting cancer growth and osteolysis through immune modulation. Results of these analyses clearly demonstrate that pDC play a key role in this vicious cascade.

From our studies, it is apparent that dissemination of the breast cancer to the bone initiates infiltration of macrophages (Fig. 2a), which produces an inflammatory response, resulting in the triggering of a pDC response (Fig. 2b). Although the signal that induces pDC accumulation has not yet been identified, it is possible that infiltration of macrophages to the site of invading cancer cells, as well as proliferating breast cancer cells in the bone microenvironment, may cause an increase in the production of Flt-3 ligand. Production of Flt-3 ligand in turn has been linked to inflammation in the bone post neoplastic breast cell infiltration (21).

Macrophage differentiation, growth and chemotaxis are regulated by many growth factors, including CSF-1, GM-CSF, IL-3 and several chemokines including MCP-1 (CCL-2) and RANTES (CCL5). MCP-1 over-expression has been reported in many cancers including breast cancer (22–25). Similarly, a significant increase in RANTES has also been reported in BM micro-environment of multiple myeloma patients (26). Results of multiplex analysis indicated a significant increase in MCP-1, RANTES, IL-3 and IL-6, suggesting a probable role of these cytokines and growth factors in macrophage infiltration (Fig. S1). Levels of pro-inflammatory cytokines were significantly reduced following pDC depletion, which correlated with an absence of bone metastasis. On the other hand IP-10, a potent inhibitor of both angiogenesis and tumor growth in the bone *in vivo* (27, 28) was upregulated in pDC depleted mice (Fig. S3) thus supporting the importance of these molecules in suppressing bone metastasis in these mice.

Another notable finding of the present study is elevated levels of pDC, Treg, Th2 and MDSC in the BM compared to that in the spleen suggesting the suppressive immune response is polarized more in the BM than in the spleen (data not shown). As pDC reside mainly in the bone, it was not surprising to note greater pDC levels in BM. However, a striking discovery in the present study was the prevalence of an increasing pDC population as cancer growth progressed in the bone. pDC activation of $CD4^+$ T cells was correlated with higher CD40 expression on pDC and higher CD40L expression on $CD4^+$ T cells along with increased IL-3 production by the $CD4^+$ T cells. This ligation was maintained throughout the period of progressive cancer burden and bone destruction, suggesting that constant stimulation of $CD4^+$ T cells by pDC is critical for skewing and maintaining the immune response towards a Th2 phenotype (29, 30). Concomitant to this effect, the levels of osteolytic cytokines IL-3, IL-6, IL-11, and IL-15 were maintained at elevated levels (31, 32).

Skewing of the immune response towards the Th2 phenotype was associated with decreased Th1 response. Elevated Th2 associated cytokines IL-13, IL-4 and IL-5 alongwith low levels of Th1 cytokines like IP-10 and IFN-γ (Fig. 3 & S3), further maintained Th2 polarization. At the initial stage of cancer dissemination (notably days 3 and 7), there was an initial spike in Th1 cells (Fig. 3). This observation suggests that although a significant Th1 response was not noted during progressive stages of breast cancer dissemination, a notable increase in Th1 cells during the first few days caused an initial influx of anti-tumor activity-inducing immune effector cells, which may have been dampened by a gradual increase in pDC and Th2 cells and associated cytokine production, facilitating immunosuppression, tumor growth and osteolysis.

It was not surprising to observe increased levels of both Treg and MDSC in the bone microenvironment. Both of these immunosuppressive cells are known to be upregulated in the presence of IL-10 and TGF-β (33). Interestingly, activated Treg were noted even at a late stage of the disease, when the overall host immune response may have been greatly dampened due to increased tumor burden. Recent studies have shown that MDSC induce immune-suppression and allow progression of several cancers including breast cancer and reduction of MDSC significantly delays primary tumor growth (34–37).

The significance of high pDC numbers and a shift in T cell homeostasis in promoting tumor growth, immunosuppression and osteolytic bone damage was further confirmed by depletion of the pDC population prior to tumor challenge. Dampening of the pDC response not only resulted in a greater decrease of tumor growth in the bone but also in other metastatic sites including lungs, and liver. Results indicated a shift from a Th2 to Th1 immune response following pDC depletion, as evidenced by an increase in IL-12 production (Fig. S3) and activated Th1 cells. Cytotoxicity assay using $CD8^+$ T cells isolated from pDC depleted mice further confirmed a direct effect on both the reversal to Th1 polarization and anti-tumor activity both in the bone and in visceral tissues, along with an increase in IFN-γ levels. Thus, it remains possible that by depleting pDC accumulation in breast cancer patients (18, 19) augmentation of anti-tumor immunity may be achieved.

Coupled to other cancer immunotherapy strategies, whether active immune response through tumor antigen-specific vaccines or treatments aimed at non-specific activation of immune effectors by passive immunotherapy including GM-CSF and IL-2 therapies, pDC depletion therapy is likely to promote an augmented anti-tumor effect and extend survival. A remarkable decrease in the production of osteolytic cytokines following pDC depletion also strongly suggests that incorporation of this unique axis into therapy regimens will improve bone remodeling significantly and decrease progressive bone loss in patients with breast cancer.

Supplementary Material

Refer to Web version on PubMed Central for supplementary material.

Acknowledgments

This work was supported in part by National Institutes of Health grants R01AR050251, 1R01AR058344-01, R01CA133737, and P30 AR046031-10 and by the U.S. Army Department of Defense grants BC044440 and BC101411.

Non-invasive imaging was carried out at UAB's Small Animal Imaging. Bone histomorphometry and micro-CT analyses were performed in UAB Bone Histomorphometry Core and Small Animal Bone Phenotyping Core, respectively. Flow cytometry analysis was performed in UAB-CFAR Core facility. We thank Enid Keyser for technical assistance in flow cytometry and sorting and the Analytical and Preparative Cytometry Facility (APCF, supported by NIH grant P30 AR48311) of the Comprehensive Arthritis, Musculoskeletal and Autoimmunity Center at UAB. Flow cytometry analysis was performed in UAB-CFAR Core facility.

References

1. Lippman ME. Breast Cancer. HARRISON'S PRINCIPLES OF INTERNAL MEDICINE. 2005; 5:516–523.
2. Roodman GD. Mechanisms of bone metastasis. N Engl J Med. 2004; 350:1655–1664. [PubMed: 15084698]
3. Mundy GR. Metastasis to bone: causes, consequences and therapeutic opportunities. Nat Rev Cancer. 2002; 2:584–593. [PubMed: 12154351]
4. Takayanagi H. Osteoimmunology and the effects of the immune system on bone. Nat Rev Rheumatol. 2009
5. Kong YY, Penninger JM. Molecular control of bone remodeling and osteoporosis. Exp Gerontol. 2000; 35:947–956. [PubMed: 11121682]
6. Bussard KM, GC, Mastro AM. The bone microenvironment in metastasis; what is special about bone? Cancer Met Rev. 2008; 27:41–55.
7. Cao QCW, Niu G, He L, Chen X. Multimodality imaging of IL-18--binding protein-Fc therapy of experimental lung metastasis. Clin Cancer Res. 2008; 14:6137–6145. [PubMed: 18829492]
8. Bernt KM, Ni S, Tieu AT, Lieber A. Assessment of a combined, adenovirus-mediated oncolytic and immunostimulatory tumor therapy. Cancer Res. 2005; 65:4343–4352. [PubMed: 15899826]
9. Chen YRS. Novel murine mammary epithelial cell lines that form osteolytic bone metastases: effect of strain background on tumor homing. Clinical and Experimental Metastasis. 2003; 20:111–120. [PubMed: 12705632]
10. Bailey-Buchtrout SL, Caulkins S, Goings G, Fischer JAA, Dzionek A, Miller SD. Cutting edge: Central nervous system plasmacytoid dendrtic cells regulate the severity of relapsing experimental autoimmune encephalomyelitis. J Immunol. 2008; 180:6457–6461. [PubMed: 18453561]
11. Chanda D, Isayeva T, Kumar S, Hensel JA, Sawant A, Ramaswamy G, Siegal GP, Beatty MS, Ponnazhagan S. Therapeutic Potential of Adult Bone Marrow–Derived Mesenchymal Stem Cells in Prostate Cancer Bone Metastasis. Clin Cancer Res. 2009; 15:7175–7185. [PubMed: 19920103]
12. Erlebacher A, Derynck R. Increased expression of TGF-beta 2 in osteoblasts results in an osteoporosis-like phenotype. J Cell Biol. 1996; 132:195–210. [PubMed: 8567723]
13. duPre' SARD, Hunter KW Jr. Microenvironment of the murine mammary carcinoma 4T1: endogenous IFN-gamma affects tumor phenotype, growth, and metastasis. Experimental and Molecular Pathology. 2008; 85:174–188. [PubMed: 18929358]
14. Palmqvist P, Lundberg P, Persson E, Johansson A, Lundgren I, Lie A, Conaway HH, Lerner UH. Inhibition of hormone and cytokine-stimulated osteoclastogenesis and bone resorption by interleukin-4 and interleukin-13 is associated with increased osteoprotegerin and decreased RANKL and RANK in a STAT6-dependent pathway. J Biol Chem. 2006; 281:2414–2429. [PubMed: 16251181]
15. Rissoan M-C, Soumelis V, Kadowaki N. Reciprocal control of T helper cell and dendritic cell differentiation. Science. 1999; 283:1183–1186. [PubMed: 10024247]

16. Muller AJ, Sharma MD, Chandler PR, Duhadaway JB, Everhart ME, Johnson BA 3rd, Kahler DJ, Pihkala J, Soler AP, Munn DH, Prendergast GC, Mellor AL. Chronic inflammation that facilitates tumor progression creates local immune suppression by inducing indoleamine 2,3 dioxygenase. Proc Natl Acad Sci U S A. 2008; 105:17073–17078. [PubMed: 18952840]
17. Asselin-Paturel C, Brizard G, Chemin K, Boonstra A, O'Garra A, Vicari A, Trinchieri G. Type I interferon dependence of plasmacytoid dendritic cell activation and migration. J Exp Med. 2005; 201:1157–1167. [PubMed: 15795237]
18. Ferrari S, Malugani F, Rovati B, Porta C, Riccardi A, Danova M. Flow cytometric analysis of circulating dendritic cell subsets and intracellular cytokine production in advanced breast cancer patients. Oncol Rep. 2005; 14:113–120. [PubMed: 15944777]
19. Treilleux IJ-YB, Bendriss-Vermare N. Dendritic cell infiltration and prognosis of early stage breast cancer. Clin Cancer Res. 2004; 10:7466–7474. [PubMed: 15569976]
20. Horny HP, Feller AC, Horst HA, Lennert K. Immunocytology of plasmacytoid T cells: marker analysis indicates a unique phenotype of this enigmatic cell. Human Pathology. 1987; 18:28–32. [PubMed: 3493197]
21. Cohen PA, KG, Czerniecki BJ, Bunting KD, Fu XY, Wang Z, Zhang WJ, Carter CS, Awad M, Distel CA, Nagem H, Paustian CC, Johnson TD, Tisdale JF, Shu S. STAT3- and STAT5-dependent pathways competitively regulate the pan-differentiation of CD34pos cells into tumor-competent dendritic cells. Blood. 2008; 112:1832–1843. [PubMed: 18577706]
22. Fujimoto HST, Ishii G, Ikehara A, Nagashima T, Miyazaki M, Ochiai A. Stromal MCP-1 in mammary tumors induces tumor-associated macrophage infiltration and contributes to tumor progression. Int J Cancer. 2009; 125:1276–1284. [PubMed: 19479998]
23. Ksiazkiewicz MGE, Kreutz M, Mack M, Hofstaedter F, Kunz-Schughart LA. Importance of CCL2-CCR2A/2B signaling for monocyte migration into spheroids of breast cancer-derived fibroblasts. Immunobiology. 2010; 215:737–747. [PubMed: 20605053]
24. Lazar MSJ, Chipitsyna G, Aziz T, Salem AF, Gong Q, Witkiewicz A, Denhardt DT, Yeo CJ, Arafat HA. Induction of monocyte chemoattractant protein-1 by nicotine in pancreatic ductal adenocarcinoma cells: role of osteopontin. Surgery. 2010; 148:298–309. [PubMed: 20579680]
25. Mishra PBD, Ben-Baruch A. Chemokines at the crossroads of tumor-fibroblast interactions that promote malignancy. J Leukoc Biol. 2010 Epub.
26. Cao YLT, Kobold S, Hildebrandt Y, Gordic M, Lajmi N, Meyer S, Bartels K, Zander AR, Bokemeyer C, Kröger N, Atanackovic D. The cytokine/chemokine pattern in the bone marrow environment of multiple myeloma patients. Exp Hematol. 2010; 38:860–867. [PubMed: 20619313]
27. Angiolillo ALSC, Taub DD, Liao F, Farber JM, Maheshwari S, Kleinman HK, Reaman GH, Tosato G. Human interferon-inducible protein 10 is a potent inhibitor of angiogenesis in vivo. J Exp Med. 1995; 182:155–162. [PubMed: 7540647]
28. Dufour JHDM, Liu MT, Leung JH, Lane TE, Luster AD. IFN-gamma-inducible protein 10 (IP-10; CXCL10)-deficient mice reveal a role for IP-10 in effector T cell generation and trafficking. J Immunol. 2002; 168:3195–3204. [PubMed: 11907072]
29. Chaperot LPI, Jacob MC, Blanchard D, Salaun V, Deneys V, Lebecque S, Brière F, Bensa JC, Plumas J. Leukemic plasmacytoid dendritic cells share phenotypic and functional features with their normal counterparts. Eur J Immunol. 2004; 34:418–426. [PubMed: 14768046]
30. Martin-Gayo E, Sierra-Filardi E, Corbi AL, Toribio ML. Plasmacytoid dendritic cells resident in human thymus drive natural Treg cell development. Blood. 2009; 115:5366–5375. [PubMed: 20357241]
31. Lebre MC, Jongbloed SL, Tas SW, Smeets TJ, McInnes IB, Tak PP. Rheumatoid arthritis synovium contains two subsets of CD83-DC-LAMP-dendritic cells with distinct cytokine profiles. Am J Pathol. 2008; 172:940–950. [PubMed: 18292234]
32. Nasrazadani A, Van Den Berg CL. c-Jun N-terminal Kinase 2 Regulates Multiple Receptor Tyrosine Kinase Pathways in Mouse Mammary Tumor Growth and Metastasis. Genes Cancer. 2011; 2:31–45. [PubMed: 21779479]

33. Jia W, Jackson-Cook C, Graf MR. Tumor-infiltrating, myeloid-derived suppressor cells inhibit T cell activity by nitric oxide production in an intracranial rat glioma + vaccination model. J Neuroimmunol. 223:20–30. [PubMed: 20452681]

34. Sinha P V, Clements K, Bunt SK, Albelda SM, Ostrand-Rosenberg S. Cross-talk between myeloid-derived suppressor cells and macrophages subverts tumor immunity toward a type 2 response. J Immunol. 2007; 179:977–983. [PubMed: 17617589]

35. Corzo CA, Condamine T, Lu L, Cotter MJ, Youn JI, Cheng P, Cho HI, Celis E, Quiceno DG, Padhya T, McCaffrey TV, McCaffrey JC, Gabrilovich DI. HIF-1alpha regulates function and differentiation of myeloid-derived suppressor cells in the tumor microenvironment. J Exp Med. 207:2439–2453. [PubMed: 20876310]

36. Cao M, Xu Y, Youn JI, Cabrera R, Zhang X, Gabrilovich D, Nelson DR, Liu C. Kinase inhibitor Sorafenib modulates immunosuppressive cell populations in a murine liver cancer model. Lab Invest.

37. Fujita M, Kohanbash G, Fellows-Mayle W, Hamilton RL, Komohara Y, Decker SA, Ohlfest JR, Okada H. COX-2 Blockade Suppresses Gliomagenesis by Inhibiting Myeloid-Derived Suppressor Cells. Cancer Res.

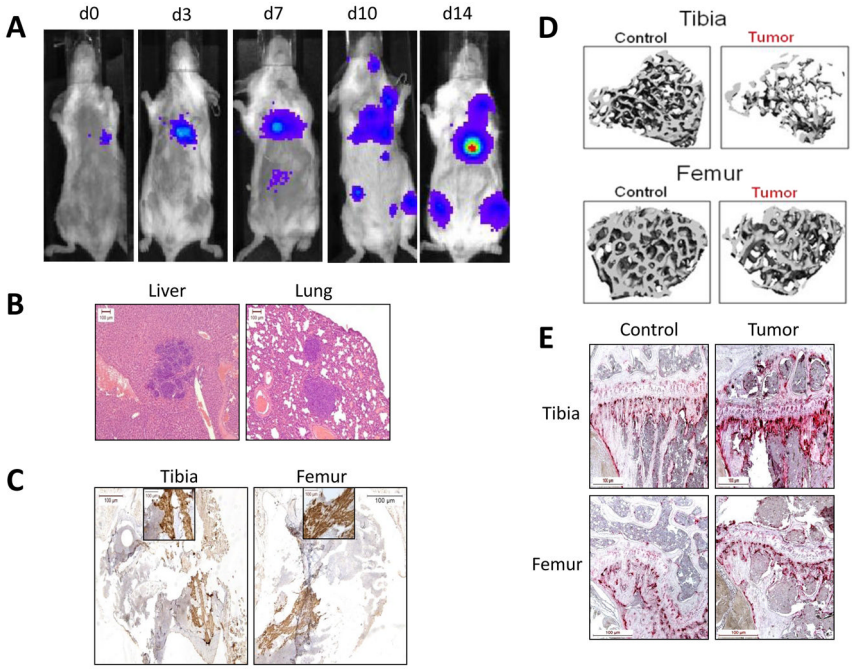

Figure 1. ***In vivo*** **model for bone metastasis of the breast cancer**

(a) The murine breast cancer cell line 4T1(fLuc) was injected into female BALB/c mice via the intra-cardiac route. Growth and spread of the tumor was followed on days 3, 7, 10 and 14 by non-invasive luciferase imaging. A representative image for each time point is shown. **(b)** Mice were sacrificed and liver and lungs were collected and paraffin sections were stained with H&E to detect the presence of tumor cells. Representative images from mice sacrificed 14 days post-tumor challenge are presented. **(c)** Cytokeratin-8 staining was performed on paraffin sections of the femur and tibia from mice 14 days after tumor challenge. Inset represents 40x image. **(d)** Fourteen days post-tumor challenge, tibia and femur were collected and subjected to Micro-CT analysis. As a control, tibia and femur from age-matched mice were included. **(e)** Paraffin sections from fourteen days post tumor-challenged mice were TRAP stained to detect osteoclasts. Six mice were used for each time point and the experiment was performed 3 times independently.

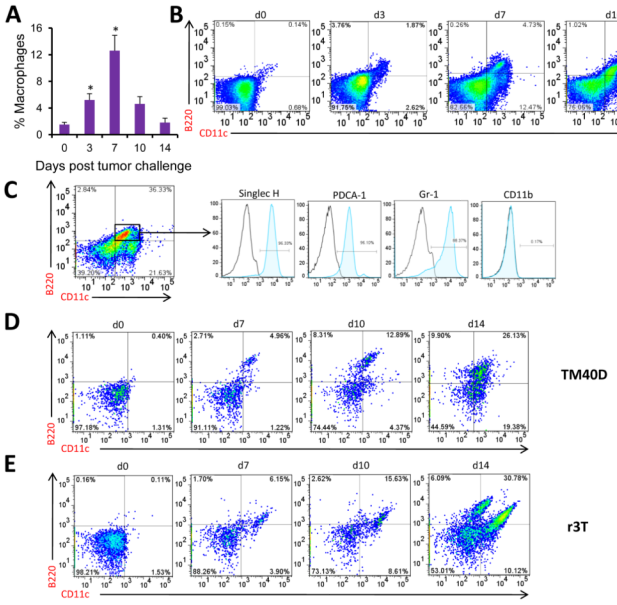

Figure 2. Numbers of pDC increase with increased dissemination of the breast cancer to bone

(a) On days 3, 7, 10 and 14 following tumor cell injection, mice were sacrificed and BM cells were isolated as mentioned in Materials and Methods. The presence of macrophages was detected using anti-F4/80 and enumerated by flow cytometry. **(b)** pDC were detected by staining with B220 and CD11c antibodies and analyzed by flow cytometry. A representative data set from each time point is shown. **(c)** Presence of pDC ($B220^{+}CD11c^{+}$) was further confirmed with Singlec-H, PDCA- 1, Gr-1 and CD11b antibodies. Data are shown for mice 14 days post-tumor challenge. **(d)** BALB/c and 129S mice were injected with TM40D and r3T cells respectively via intra- cardiac route. pDC levels were evaluated by flow cytometry using B220 and CD11c, antibodies on days 7, 10 and 14 from BM, similar to that described above. Representative data from each time point for both the cell lines is provided here. Bone marrow cells were isolated from 6 mice for every time point and were treated as individual samples. For each sample, the above mentioned flow cytometry analysis was performed. This experiment was performed three times independently.

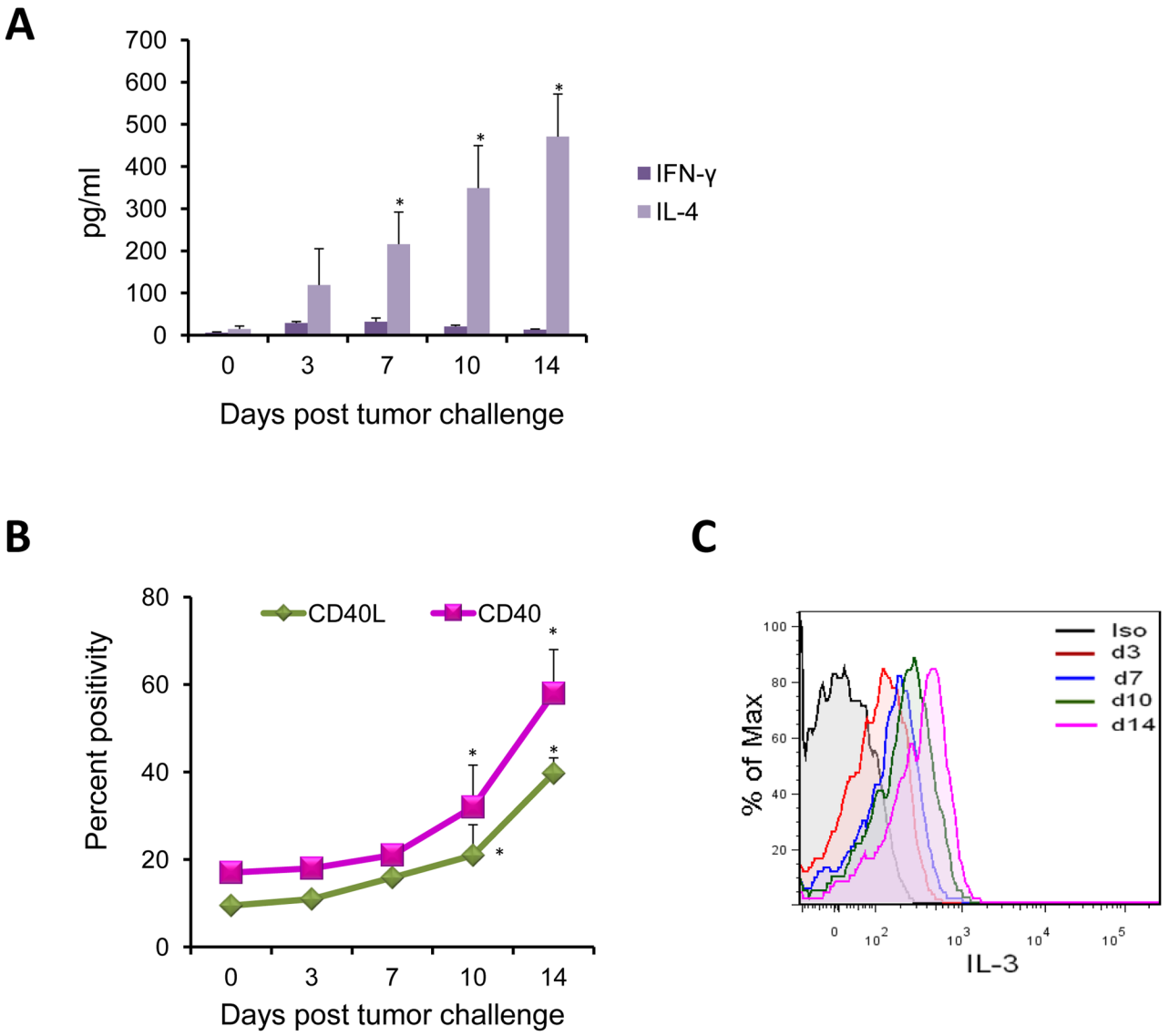

Figure 3. Elevation in pDC is concomitant with elevation in Th2 cells

(a) Serum samples from mice on days 3, 7, 10 and 14 post-tumor challenge were assayed for levels of IFN-γ and IL-4 by multiplex ELISA as per the manufacturer's instructions. Results are expressed as pg/ml of respective cytokine ± SE (N=3, *p<0.05). **(b)** Cells stained for pDC and $CD4^+$ T cell markers were stained for CD40 and CD40L respectively. Results are shown as percent positivity in the expression of these markers compared to control. **(c)** Cells isolated from BM were cultured in RPMI-1640 in the presence of 5 ng/ml PMA, 500 ng/ml Ionomycin and 1 μg/ml GolgiPlug protein transport inhibitor for 4 hrs. Cells were then stained with surface antibodies to CD3 and CD4. Upon permeabilization, cells were stained with antibody to IL-3. Percent of IL-3 secreting CD^+ T cells was analyzed by flow cytometry by intra-cellular staining. Data is a representative curve at each time point. Statistical analysis included N=3, *p<0.05 by Student's t-test. Six mice were included for each time point and the experiment was repeated three times independently.

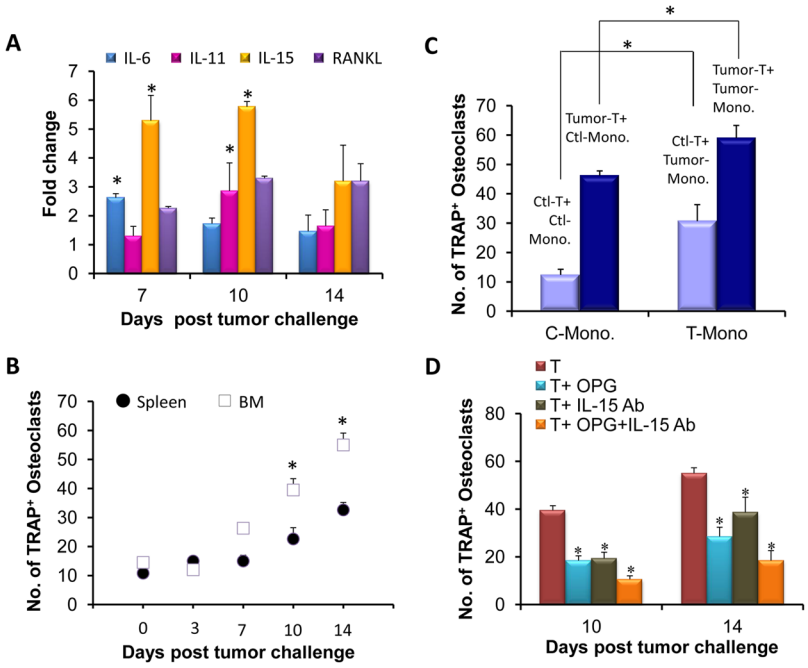

Figure 4. RANKL and IL-15 antagonist decrease osteoclast activity during bone metastasis of the breast cancer cells

(a) RNA was isolated from BM $CD4^+$ T cells, cDNA was synthesized and used in real-time RT-PCR analysis for IL-6, IL-11, IL-15 and RANKL. Data is presented as fold change in the expression of RNA as compared to the control. **(b)** Monocytes and $CD4^+$ T cells isolated from BM and spleen were co-cultured in a ration of 1:100, respectively, for osteoclast differentiation. Cells with 3 or more nuclei were scored as osteoclasts following TRAP staining. **(c)** Monocytes isolated on day 14 from tumor-challenged mice were co-cultured with $CD4^+$ T cells from either the tumor-challenged or the control mice for osteoclast differentiation. **(d)** On days 10 and 14, OPG or antibody to IL-15 was added to the co-cultures of monocytes and $CD4^+$T cells individually or in combination. After 10 days, TRAP staining was performed to detect the presence of osteoclasts. For statistical analysis, N=3, *$p<0.05$ by Student's t-test. The above experiments were performed by isolating cells from 6 different mice for each time point. The experiments were repeated 3 times independently.

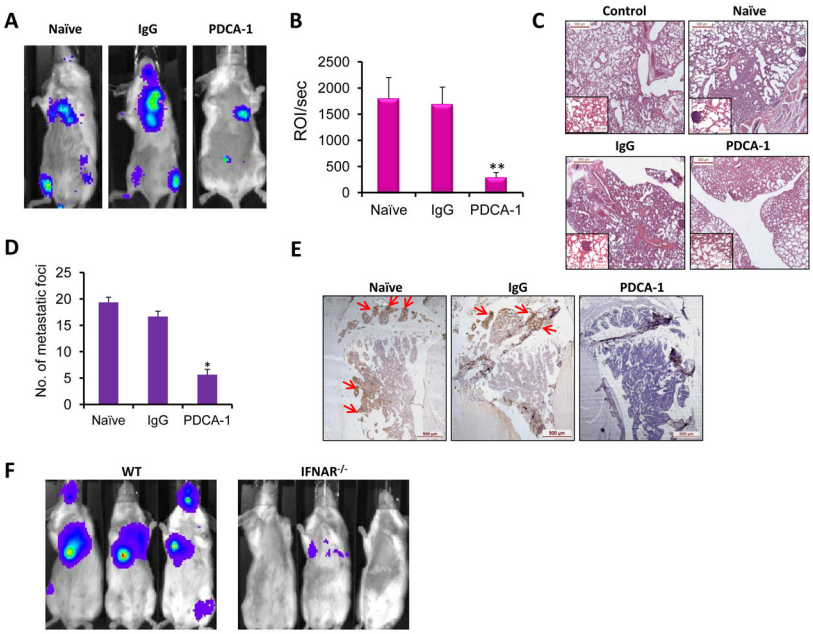

Figure 5. Depletion of pDC significantly reduces the growth of the breast cancer cells *in vivo*

(a) Representative luciferase imaging of naïve, IgG-treated and PDCA-1-treated mice twelve days after tumor challenge are presented. **(b)** Total luciferase counts from mice of each group, 12 days post tumor challenge are presented. **(c)** Paraffin section of lungs from naïve, IgG injected and PDCA-1 injected mice were stained with H&E. A representative section from each group is shown. Inset represents 20x magnification. **(d)** Breast cancer metastasis sites in the lungs were counted for naïve, IgG injected and PDCA-1 injected mice. **(e)** Paraffin sections of tibia from naïve, IgG- and PDCA-1-treated mice were stained with cytokeratin-8 antibody. Arrows indicate presence of breast cancer cells on the section. **(f)** Representative luciferase imaging of 4T1(fLuc) cell-challenged WT and IFNAR$^{-/-}$ mice (BALB/c background) 12 days post tumor challenge are shown. Statistical analysis included N=3, *p<0.05, **p<0.01 by Student's t-test. Depletion of pDC was performed twice independently. For each time point, 3 mice were included in naïve, IgG and PDCA-1 groups.

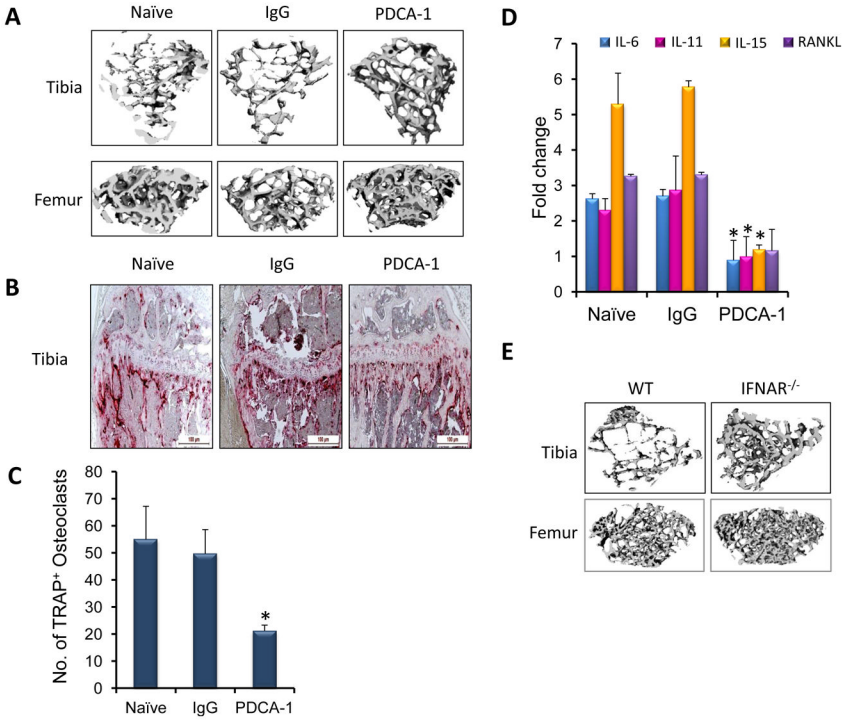

Figure 6. Decreased numbers of osteoclasts results in the absence of bone destruction in pDC depleted mice

(a) Twelve days post-tumor challenge, tibia and femur from naïve, IgG-and PDCA-1-treated group were subjected to micro-CT analysis. **(b)** Paraffin sections of tibia from the naïve, IgG injected and PDCA-1 injected mice twelve days after tumor challenge were stained for TRAP to detect osteoclasts. **(c)** On day 12 post tumor challenge, monocytes and $CD4^+$T cells from naïve, IgG and PDCA-1 antibody injected mice were co-cultured to assay osteoclast numbers. **(d)** cDNA from $CD4^+$T cells of naïve, IgG- and PDCA-1 antibody treated mice were used to detect the levels of IL-6, IL-11, IL-15 and RANKL by real-time RT-PCR. Data is presented as a fold change in expression of RNA compared to the control. **(e)** Micro-CT analysis of tibia and femur from WT and $IFNAR^{-/-}$ mice 12 days post tumor challenge. For statistical analysis, N=3, *$p<0.05$ by Student's t-test. Presented data is from 3 different mice from each group. These experiments were repeated twice separately.

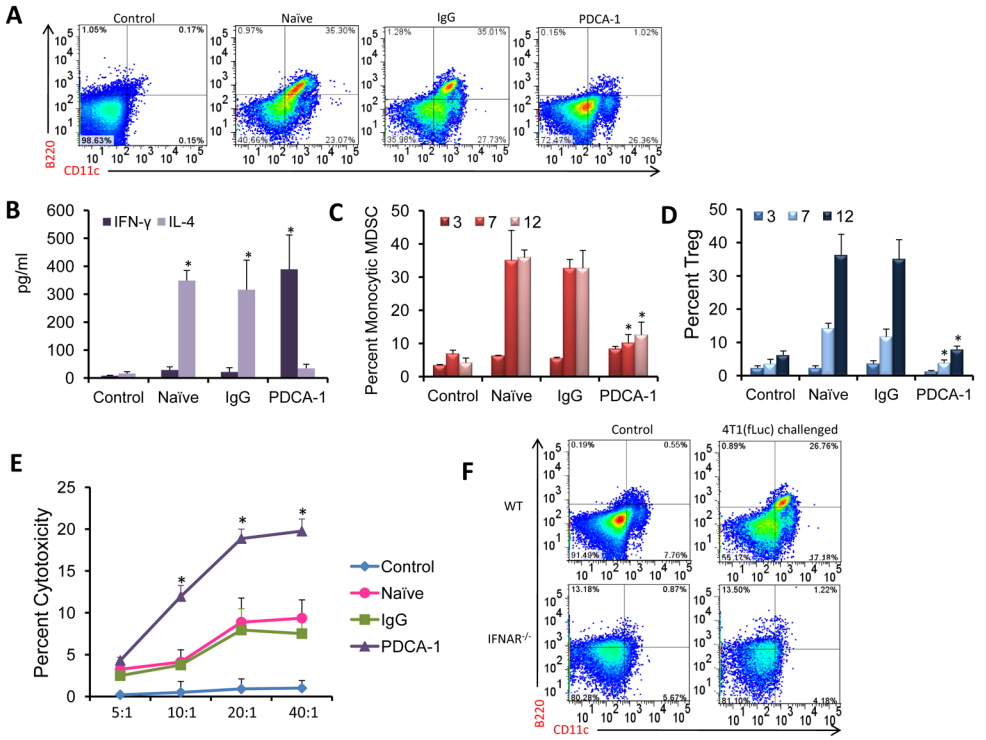

Figure 7. Depletion of pDC skews the immune response towards Th1 and results in decreased immunosuppression

(a) Presence of pDC was detected in BM from naïve, IgG and PDCA-1 antibody injected mice 12 days post tumor challenge. A representative image from the 3 groups is presented. **(b)** IFN-γ and IL-4 levels were measured as mentioned before. **(c)** Numbers of monocytic MDSC ($CD11b^{+}Ly6C^{+}Ly6G^{lo}$) in the BM after pDC depletion was enumerated by flow cytometry. **(d)** The presence of Treg cells was detected by staining BM cells from control, IgG and PDCA-1 antibody treated mice. **(e)** $CD8^{+}$ T cells isolated from the BM of IgG and PDCA-1 treated animals 3 days post tumor challenge were used as the effector population (E) with 4T1(fLuc) cells as the target population (T). Cytotoxicity assay was carried out using a commercially available kit. **(f)** Presence of pDC was detected in BM from WT and $IFNAR^{-/-}$ mice 12 days post tumor challenge. Mice with no tumor challenge included as the control group. A representative image for each group, showing percent of pDC, is presented. Statistical analysis included N=3, *p<0.05 by Student's t-test. The flow cytometry and cytotoxicity assays were from 3 mice for each group and for each time point. The experiments were repeated twice independently.